Research Square

Preprints are preliminary reports that have not undergone peer review.
They should not be considered conclusive, used to inform clinical practice,
or referenced by the media as validated information.

Macrophage-Derived Migrasomes Promote Fibrosis Remodeling in Endometriosis Through TGF-β/Smad Signaling

Ye Pan
Jiangsu University
Jie Fang
Affiliated Hospital of Jiangsu University
Simeng Zhang
Jiangsu University
Yongbing Ma
mayongbin2009@163.com
Jintan People's Hospital
Peng Lü
Jiangsu University

Research Article

Keywords: Migrasomes, Endometriosis, Macrophage, fibrosis, TGF-β/Smad signaling pathway

Posted Date: April 8th, 2026

DOI: https://doi.org/10.21203/rs.3.rs-9209859/v1

License: This work is licensed under a Creative Commons Attribution 4.0 International License.
Read Full License

Additional Declarations: No competing interests reported.

Abstract

Background

Progressive fibrosis of ectopic lesions is a major pathological feature of endometriosis, contributing to treatment resistance and disease recurrence. However, the mechanisms driving this fibrotic process remain incompletely understood.

Methods

A murine model of endometriosis was established by transplanting endometrial tissue fragments into the peritoneal cavity of C57BL/6 mice. Macrophage-derived migrasomes were isolated from cultured RAW264.7 cells, characterized by scanning electron microscopy and Western blot, and administered intraperitoneally to endometriosis-bearing mice. Fibrotic changes were assessed by histology, immunofluorescence, and Western blot analysis of signaling pathways and epithelial-mesenchymal transition (EMT) markers. Cytokine levels were measured by enzyme-linked immunosorbent assay (ELISA).

Results

Exogenously administered macrophage-derived migrasomes accumulated at ectopic lesion sites and markedly aggravated fibrotic remodeling. Migrasome-treated lesions exhibited cyst-wall thickening, increased stromal cellularity, and extensive collagen deposition. At the molecular level, migrasome treatment was associated with activation of the transforming growth factor-beta (TGF-β)/Smad pathway in ectopic lesions, as indicated by increased phosphorylation of Smad2 and Smad3 without significant changes in total Smad2/3 levels. This was accompanied by increased α-smooth muscle actin and vimentin expression together with reduced cytokeratin 18 (CK18) and E-cadherin expression, consistent with EMT-like phenotypic reprogramming. In parallel, TGF-β1 and VEGF levels were elevated, whereas MMP9 was reduced, collectively supporting a pro-fibrotic microenvironment.

Conclusions

These findings identify macrophage-derived migrasomes as previously unrecognized promoters of fibrotic remodeling in endometriosis and support a role for migrasome-associated signaling in lesion progression. This work provides new insight into the pathogenesis of endometriosis-associated fibrosis and highlights migrasomes as a potential target for future anti-fibrotic intervention.

Plain English summary

Endometriosis happens when tissue similar to the lining of the uterus grows outside the uterus, often causing pain and fertility problems. Over time, these growths can become thickened and scarred, a process called fibrosis, which can make the disease harder to treat and more likely to recur. However, scientists do not fully understand what causes this scarring. In this study, we investigated whether migrasomes—small membrane-bound structures released by moving cells—contribute to this scarring process.

Using a mouse model of endometriosis, we found that migrasomes derived from macrophages, a type of immune cell, could reach the lesion sites and remain there for several days. Their presence was associated with thicker lesion walls, more collagen buildup, and a more fibrotic tissue structure. We also found that migrasome treatment was linked to activation of the TGF-β/Smad pathway, a signaling pathway well known to be involved in scarring, together with changes in cell markers consistent with a shift toward a more mesenchymal, fibrosis-prone state.

These findings suggest that macrophage-derived migrasomes may help promote fibrosis in endometriosis. By identifying this previously underappreciated mechanism, our study provides a new way of thinking about how endometriosis lesions become progressively scarred and difficult to treat, and it points to migrasomes as a potential target for future therapies.

Introduction

Endometriosis (EMS) is a prevalent, estrogen-dependent chronic inflammatory disorder, charactered by the presence of endometrial-like tissue outside the uterine cavity [1]. It affects approximately 5–10% of women of reproductive age, leading to debilitating symptoms such as chronic pelvic pain, infertility, and the formation of fibrotic lesions that significantly compromise life quality [2–4]. Although first-line interventions, including laparoscopic surgery combined with gonadotropin-releasing hormone agonist (GnRH-a) therapy, provide temporary symptomatic relief [5–8], fibrosis-induced adhesions and high postoperative recurrence rates remain major clinical challenges [9].

Pathological fibrosis in EMS is characterized by excessive extracellular matrix (ECM) deposition and aberrant tissue remodeling [10]. This process is driven by multiple cellular phenotypic transitions, including epithelial-mesenchymal transition (EMT), fibroblast-to-myofibroblast transdifferentiation (FMT), and endothelial-to-mesenchymal transition (EndoMT) [11]. FMT is considered a major source of α-smooth muscle actin (α-SMA)-positive myofibroblast-like cells, which serve as key effectors of ECM production [12]. In parallel, EMT enhances the migratory and invasive properties of ectopic endometrial cells [13], whereas EndoMT contributes to mesenchymal expansion by facilitating phenotypic conversion of microvascular endothelial cells [14]; collectively, these processes promote fibrotic progression. The tumor-like microenvironment of EMS lesions, particularly the immune cell infiltrate, plays a critical role in orchestrating these events [15].

Among infiltrating immune cells, macrophages are pivotal regulators of the EMS microenvironment [16]. Macrophages in EMS lesions often exhibit an M2-like, pro-fibrotic bias [17]. and secrete a range of

mediators, including transforming growth factor-β (TGF-β) [18], platelet-derived growth factor (PDGF) [19], and connective tissue growth factor (CTGF) [20]. These mediators activate canonical signaling pathways, including Smad signaling, and promote FMT, EMT, and ECM synthesis and cross-linking [21]. Single-cell RNA sequencing studies have further revealed close spatial interactions between macrophages and myofibroblast-like stromal populations in EMS lesions, underscoring the importance of intercellular communication in lesion remodeling [22]. However, the traditional paradigm of paracrine signaling by soluble factors may be insufficient to explain the persistence and specificity of fibrotic progression.

Migrasomes are a recently discovered class of migration-associated extracellular vesicular structures that form at the tips of retraction fibers and are subsequently released into the extracellular space [23]. These large vesicular structures are characterized by enrichment of tetraspanin family proteins, such as TSPAN4, and can carry diverse bioactive molecules, including proteins, nucleic acids, and enzymes [24–27]. Emerging evidence has established critical roles for migrasomes in embryonic development, immune regulation, and cancer metastasis [28, 29]. Notably, a recent study in sepsis-induced pulmonary fibrosis showed that neutrophil-derived migrasomes, after uptake by macrophages, could promote fibrogenesis by triggering macrophage-to-myofibroblast transition (MMT) through mitochondrial DNA transfer [30]. These findings suggest that migrasomes may represent previously underappreciated mediators of fibrotic remodeling. Nevertheless, their existence, lesion association, and functional relevance in EMS-associated fibrosis remain unknown.

Based on this background, we hypothesized that macrophage-derived migrasomes contribute to EMS fibrosis by engaging pro-fibrotic signaling pathways such as TGF-β/Smad, thereby promoting fibrotic remodeling and EMT-like phenotypic shifts. To address this hypothesis, we first examined the presence of TSPAN4-positive migrasome-like structures in ectopic lesions and their spatial relationship with infiltrating macrophages in a murine model of EMS. We then isolated macrophage-derived migrasomes in vitro and evaluated their effects on lesion remodeling, EMT-like phenotypic changes, and TGF-β/Smad pathway activation *in vivo*. Our findings support a previously unrecognized role for macrophage-derived migrasomes in EMS-associated fibrosis and provide a new perspective on the microenvironmental mechanisms that underlie fibrotic progression.

Results

TSPAN4-positive migrasome-like structures are detected in ectopic lesions and show spatial association with infiltrating macrophages

A murine model of endometriosis was established by transplanting endometrial tissue fragments into the peritoneal cavity of C57BL/6 mice, resulting in ectopic lesions adherent to the abdominal wall (Fig. 1B). Both donor and recipient mice in estrus were selected for the experiment, as verified by vaginal

cytology showing a predominance of cornified epithelial cells (Fig. 1A). Macroscopic examination performed four weeks after transplantation revealed cystic lesions characteristic of ectopic endometrial growth.

Within these ectopic lesions, distinct TSPAN4-positive structures were readily detected by immunofluorescence analysis, predominantly localized to the perilesional and stromal compartments. TSPAN4, a hallmark membrane protein of migrasomes, displayed a punctate and vesicular distribution pattern consistent with migrasome morphology.

The cellular origin of these TSPAN4-positive structures was subsequently examined through multiplex immunofluorescence co-localization analysis. CD163 and CD86 were selected as representative markers frequently associated with M2-like anti-inflammatory/pro-repair and M1-like pro-inflammatory macrophage phenotypes, respectively. Notably, TSPAN4 signals exhibited extensive spatial overlap with both CD163- and CD86-positive cells (Fig. 1C, E), indicating a close association between migrasomes and infiltrating macrophage populations. Quantitative colocalization analysis using Manders' overlap coefficients further substantiated this observation, yielding coefficients of 0.78 ± 0.04 for TSPAN4/CD163 and 0.71 ± 0.05 for TSPAN4/CD86 (Fig. 1D, F). Together, these findings indicate that migrasome-like structures are present within ectopic lesions and are closely associated with infiltrating macrophages across distinct phenotypic states.

Isolation and structural characterization of macrophage-derived migrasomes

Macrophage-derived migrasomes were collected from conditioned medium of cultured macrophages through sequential isolation and purification, yielding sufficient material for subsequent functional analyses (Fig. 2A). The morphology of the isolated vesicles was examined by scanning electron microscopy (SEM). The preparations contained abundant large vesicular structures with diameters of approximately 1–3 μm, consistent with the reported size range of migrasomes. These vesicles displayed characteristic migrasome-like morphology, including rounded membrane-bound structures connected to elongated membranous extensions (Fig. 2B), indicating that the isolation procedure preserved migrasome ultrastructural integrity.

The molecular identity of the isolated vesicles was further evaluated by Western blot analysis. The preparations showed detectable enrichment of established migrasome-associated proteins, including the tetraspanin TSPAN4 and the glycosyltransferases EOGT and PIGK (Fig. 2C). Together, these structural and molecular features support the successful isolation of macrophage-derived migrasome-enriched preparations for downstream *in vivo* and mechanistic studies.

Macrophage-derived migrasomes exacerbate fibrotic remodeling of endometriotic lesions

To determine whether exogenously administered macrophage-derived migrasomes could access ectopic lesions *in vivo*, isolated migrasomes were labeled with DiR and intraperitoneally injected into mice bearing established endometriotic cysts (Fig. 3A). Longitudinal whole-body imaging revealed a clear accumulation of fluorescence signals at lesion sites in the DiR-migrasome group, whereas only weak and diffuse background signals were detected in the DiR control group (Fig. 3C). Quantification of lesion-associated fluorescence demonstrated sustained high signal intensity during the initial four days, followed by a gradual decline thereafter (Fig. 3D). Ex vivo analysis at endpoint confirmed significantly higher fluorescence intensity in endometriotic cysts compared to major organs, further supporting lesion-associated accumulation and retention (Fig. 3E). This kinetic profile supports efficient lesion accumulation with prolonged local retention and guided the subsequent dosing regimen, in which migrasomes were administered at four-day intervals to interrogate their functional impact on lesion progression (Fig. 3B).

After four consecutive administrations of migrasomes, gross inspection at the experimental endpoint uncovered striking macroscopic differences in lesion appearance. Control cysts were typically translucent, with thin walls and clear intracystic fluid. By contrast, lesions from migrasome-treated mice displayed a greyish-brown coloration and markedly thickened, opaque cyst walls (Fig. 3G), suggesting enhanced tissue remodeling. Notably, no difference in body weight was observed between the two groups (Fig. 3F), and cyst size was not significantly different (Migrasome group: 7.18 ± 0.26 mm vs. Control group: 7.86 ± 0.63 mm, $p > 0.05$; Fig. 3H), indicating that migrasome exposure altered lesion architecture rather than overall lesion size.

Histopathological analyses (performed as outlined in Fig. 4A and 4C) corroborated a pronounced shift toward a pro-fibrotic lesion phenotype. Hematoxylin and eosin (H&E) staining revealed markedly thickened cyst walls accompanied by increased stromal cellularity, altered tissue architecture, and prominent inflammatory cell infiltration in migrasome-treated lesions (Fig. 4B). Consistent with these structural changes, Masson's trichrome staining demonstrated extensive and confluent collagen deposition throughout the stromal compartment of migrasome-treated cysts, whereas control lesions displayed only sparse and discontinuous collagen fibers (Fig. 4D). Morphometric quantification confirmed a striking increase in fibrotic area in the migrasome-treated group compared with controls (56.0% ± 0.6% vs. 4.97% ± 0.07%, $p < 0.0001$; Fig. 4E). Together, these findings indicate that intraperitoneally delivered macrophage-derived migrasomes accumulate at lesion sites and promote a pronounced fibrotic remodeling program characterized by stromal expansion and extensive collagen deposition.

Migrasomes induce EMT-like phenotypic reprogramming in ectopic lesions

The pronounced fibrotic remodeling observed in migrasome-treated lesions led us to investigate whether migrasome exposure was accompanied by epithelial–mesenchymal transition (EMT)-like phenotypic

changes. Immunofluorescence analysis of ectopic cyst tissues (Fig. 5A) revealed coordinated alterations in epithelial and mesenchymal marker expression following migrasome treatment.

Among mesenchymal markers, vimentin expression was minimal in control lesions but was markedly increased in migrasome-treated cysts, where strong signals were observed along the cyst wall and stromal-like compartment (Fig. 5B, C), indicating expansion of mesenchymal-like cellular components within the lesion.

Concomitantly, epithelial markers were significantly suppressed. CK18 and E-cadherin expression levels were reduced to approximately 64% and 54% of control levels, respectively, corresponding to decreases of ~ 36% and ~ 46% (Fig. 5D–G). Reduced E-cadherin staining in migrasome-treated lesions further supported loss of epithelial characteristics.

Together, these reciprocal changes—upregulation of the mesenchymal marker vimentin and downregulation of epithelial markers CK18 and E-cadherin—indicate that macrophage-derived migrasomes promote EMT-like phenotypic reprogramming within ectopic endometriotic lesions.

Migrasomes engage TGF-β/Smad signaling to promote fibrotic progression

Comparable protein loading and integrity across samples were first confirmed by SDS–PAGE followed by Coomassie Brilliant Blue staining (Fig. 6A, B), which showed highly similar banding patterns between migrasome-treated and control lesion extracts, and supported the reliability of subsequent immunoblot analyses.

Analysis of fibrotic-related signaling pathways revealed robust engagement of the canonical TGF-β/Smad axis in migrasome-treated lesions. Western blot analysis showed that p-Smad2 and p-Smad3 levels were increased by 1.8-fold and 2.7-fold, respectively, in migrasome-treated lesions relative to controls ($p < 0.01$), while Smad2 and Smad3 levels remained unchanged (Fig. 6C–F). This selective enhancement of Smad phosphorylation indicates activation of TGF-β/Smad signaling at the post-translational level.

Engagement of the TGF-β/Smad pathway was associated with a coordinated pro-fibrotic shift in the lesion microenvironment. α-Smooth muscle actin (α-SMA), a marker commonly associated with contractile stromal activation and myofibroblast-like phenotypes, was significantly increased (1.67-fold, $p < 0.01$; Fig. 6G), suggesting an expansion of α-SMA–positive stromal populations with enhanced matrix-remodeling capacity. In parallel, levels of active TGF-β1 were markedly elevated (11.8-fold), as determined by ELISA (Fig. 6H), consistent with sustained upstream profibrotic signaling (Fig. 6I).

This matrix-accumulating milieu was further accompanied by increased vascular endothelial growth factor (VEGF, 1.6-fold) and a pronounced reduction in the matrix-degrading enzyme MMP9 (reduced to 27.8% of control levels; $p < 0.01$) (Fig. 6J, K). Although VEGF is primarily linked to angiogenesis, its

elevation may support lesion persistence and remodeling by facilitating vascular support within the fibrotic niche. Collectively, these molecular changes support a pro-fibrotic state characterized by activation of TGF-β/Smad signaling, increased stromal activation, and extracellular matrix accumulation in migrasome-treated lesions.

Discussion

In the present study, we identified TSPAN4-positive migrasome-like structures within ectopic lesions of a murine endometriosis model and found that macrophage-derived migrasomes were associated with fibrotic remodeling of these lesions. Endometriosis is widely recognized as a chronic inflammatory disorder characterized by repeated tissue injury, repair, and stromal remodeling, with macrophages playing central roles in lesion maintenance, angiogenesis, and fibrosis [31–34]. Previous work has largely interpreted macrophage involvement through the lens of infiltration and polarization states, particularly the balance between M1- and M2-like phenotypes [34]. Our findings extend this framework by demonstrating the presence of TSPAN4-positive punctate/vesicular structures within lesional tissues that exhibit spatial proximity or overlap with CD163- and CD86-positive macrophages. Although these colocalization data support a close association between migrasome-like structures and infiltrating macrophages, they do not establish exclusive cellular origin, as migrasomes can be generated by multiple migratory cell types [23, 35]. The functional arm of the study was therefore designed to test whether migrasomes derived from cultured macrophages are sufficient to drive fibrotic remodeling *in vivo*.

Migrasomes are formed during cell migration and can be deposited as relatively stable vesicular structures within local tissues [23]. This property of local deposition offers a conceptual framework for understanding the focal and progressive nature of fibrosis in endometriosis. Unlike soluble factors that diffuse rapidly within the peritoneal cavity, migrasomes tend to be retained in the peri-lesional microenvironment, allowing their bioactive cargo to accumulate and exert sustained local effects [36]. In endometriotic lesions, continuous macrophage infiltration and dynamic interactions with stromal cells, epithelial-like cells, and the extracellular matrix create a permissive microenvironment for tissue remodeling [37]. Within this context, the presence of migrasome-like structures suggests that macrophage migration may contribute to microenvironmental remodeling through locally deposited migrasomes [38]. Consistent with this interpretation, our *in vivo* tracing experiments showed that intraperitoneally administered macrophage-derived migrasomes could access ectopic lesions and remain detectable for several days. A more conservative interpretation is therefore that migrasomes can reach and persist within lesion sites, potentially providing sustained local stimuli for tissue remodeling, rather than that they exhibit a specific homing mechanism [36].

At the morphological level, the most prominent finding of this study was that migrasome treatment significantly enhanced lesional fibrotic remodeling. Although body weight and cyst diameter did not differ between groups, migrasome-treated lesions exhibited marked thickening of the cyst wall, increased stromal cellularity, and more compact tissue architecture. Consistent with these changes,

Masson's trichrome staining revealed extensive and confluent collagen deposition in migrasome-treated cysts, whereas control lesions displayed only sparse and discontinuous collagen fibers. Morphometric analysis confirmed a significant increase in fibrotic area in the migrasome-treated group. Collectively, these findings indicate that the primary impact of migrasomes is not to promote gross lesion expansion, but rather to alter tissue composition and architecture, shifting lesions toward a collagen-rich and stroma-expanded fibrotic phenotype. These findings also suggest that lesion size alone may underestimate substantive changes in stromal remodeling and fibrotic progression in experimental endometriosis.

At the molecular level, our data implicate the TGF-β/Smad axis in migrasome-associated fibrotic remodeling. TGF-β signaling is recognized as a central regulatory pathway in various fibrotic diseases and in endometriosis-associated stromal remodeling [32–34]. In the present study, migrasome-treated lesions exhibited significantly increased phosphorylation of Smad2 and Smad3 without changes in total Smad2/3 levels, indicating pathway activation at the post-translational level. Consistent with this, α-SMA levels were upregulated, which together with histological evidence of cyst wall thickening, stromal compaction, and collagen accumulation, this supports an interpretation of enhanced α-SMA-positive stromal/myofibroblast-like activity rather than simply reflecting increased myofibroblast numbers per se [30]. Furthermore, migrasome treatment elevated levels of active TGF-β1 and VEGF while markedly reducing MMP9 expression, collectively pointing toward a shift in ECM dynamics favoring enhanced synthesis/deposition over degradation [39, 40]. These molecular changes provide a mechanistic basis for the extensive collagen accumulation observed by Masson's trichrome staining. Although VEGF is primarily associated with angiogenesis, its upregulation in a chronic inflammatory and fibrotic microenvironment may promote vascular support for sustained cellular infiltration and tissue remodeling, thereby synergistically amplifying fibrotic progression [38]. Overall, the concordance between pathway activation, ECM regulatory factor modulation, and histological fibrotic phenotype supports the view that migrasomes contribute to pro-fibrotic microenvironmental remodeling in endometriotic lesions.

At the cellular phenotype level, migrasome-treated lesions exhibited increased vimentin expression accompanied by decreased CK18 and E-cadherin levels, reflecting a shift toward diminished epithelial characteristics and enhanced mesenchymal features. Previous studies and reviews have documented the presence of EMT/EMT-like changes, or more broadly epithelial–mesenchymal plasticity (EMP), in endometriotic lesions, typically characterized by downregulation of epithelial markers (e.g., E-cadherin, cytokeratins) and concomitant upregulation of mesenchymal markers (e.g., vimentin) [41–43]. Importantly, the literature favors interpreting these changes as partial EMT/phenotypic shift rather than complete transdifferentiation of epithelial cells into mesenchymal cells: cells retain some epithelial properties while acquiring mesenchymal-associated features, thereby enhancing migratory capacity, matrix remodeling, and lesion persistence, which in turn synergize with fibrotic remodeling [44]. Within this framework, the observed reduction in CK18 and E-cadherin suggests diminished epithelial features and cell–cell adhesion, while increased vimentin indicates expansion of mesenchymal-like components. These data therefore support an association between migrasome exposure and EMT-like phenotypic

reprogramming, or stromalization, within lesions, without implying complete lineage conversion. Future studies incorporating lineage tracing, spatial/single-cell transcriptomics, and receptor cell-type validation will help identify the primary cellular targets of migrasomes and quantify the contribution of EMT-like changes to fibrotic progression.

In addition, exploratory transcriptomic profiling suggested broad remodeling of ECM-, adhesion-, and microenvironment-associated gene programs in migrasome-treated lesions. Enrichment analyses highlighted Gene Ontology terms related to extracellular matrix organization, cell-substrate adhesion, connective tissue development, and TGF-β receptor signaling, as well as KEGG pathways including ECM-receptor interaction, TGF-β signaling, and PI3K-Akt signaling. These findings are broadly consistent with the fibrotic phenotype observed histologically. However, because of RNA quality limitations, these transcriptomic data were interpreted as exploratory and were not used as primary mechanistic evidence (Supplement).

Several limitations of this study should be acknowledged. First, although we assessed the effects of exogenously administered macrophage-derived migrasomes on established lesions, the production dynamics, spatial distribution, and stage-dependent contributions of endogenous migrasomes during natural disease progression remain to be systematically characterized. Second, while we observed activation of the TGF-β/Smad axis and coordinated changes in fibrosis-associated molecular profiles, the current study lacks pathway inhibition or rescue experiments; therefore, causal dependence of migrasome-induced fibrotic effects on this pathway cannot yet be established. Third, the key molecular cargo of migrasomes and their primary recipient cell types within lesions remain unidentified. At present, our data support an association between migrasomes and fibrotic remodeling rather than defining a precise mechanism mediated by delivery of a specific factor.

Future investigations should address these gaps through several complementary approaches. Systematic proteomic, lipidomic, and nucleic acid analyses will help define migrasome molecular composition and identify candidate effector molecules [45]. Cell-type-specific tracing, in situ co-localization, and uptake experiments will clarify the primary target cell populations and sites of migrasome action within lesions [46]. Functional validation studies using TGF-β receptor inhibition or Smad pathway interference will test the necessity of this axis in migrasome-mediated fibrotic remodeling. Finally, confirmation of migrasome–fibrosis associations in more clinically relevant systems —such as human samples, organoids, or alternative *in vivo* models—will be essential to assess reproducibility and translational potential.

In summary, this study proposes and provides supporting evidence for a "macrophage–migrasome–fibrotic remodeling" framework in the endometriotic systemic levels (Fig. 7). Migrasome-like structures are detectable within endometriotic lesions and exhibit spatial association with infiltrating macrophages. Exogenous macrophage-derived migrasomes administered intraperitoneally can access and persist within lesion sites, inducing pronounced collagen deposition and stromal remodeling accompanied by activation of the TGF-β/Smad axis and EMT-like phenotypic shifts. These findings provide new insights

into the focal and progressive nature of endometriosis-associated fibrosis and lay a foundation for future studies aimed at characterizing migrasome molecular cargo, identifying recipient cell populations, and exploring potential interventional targets.

Methods

Animals

Female C57BL/6J mice (7–8 weeks old upon arrival) were purchased from the Experimental Animal Center of Jiangsu University. Mice were housed under specific pathogen-free (SPF) conditions in individually ventilated cages (IVCs), with a 12-hour light/dark cycle, room temperature maintained at 22 ± 1°C, and relative humidity at 50 ± 10%. Standard rodent diet and autoclaved water were provided ad libitum. Bedding was changed twice weekly. All mice were acclimatized for at least 7 days before any experimental procedures. The estrous cycle was monitored by daily vaginal smear cytology, and only mice in the estrus phase (as characterized by predominant cornified epithelial cells, n = 30) were used for endometriosis model induction. Postoperative analgesia was provided to alleviate pain. Predefined humane endpoints were implemented to minimize distress.

Endometriosis model establishment

The mouse model of endometriosis was established by surgical transplantation of isolated endometrial tissues with minor modifications to previously described procedures. Anesthesia was induced and maintained with isoflurane. Mice were anesthetized in an induction chamber with 3–5% isoflurane in oxygen (flow rate, 0.5–1 L/min) and subsequently maintained with 1.5–2.5% isoflurane delivered through a nose cone during surgery. Donor uterine horns were aseptically removed under deep anesthesia, placed in sterile PBS, and opened longitudinally. The endometrial layer was then carefully separated from the uterine wall under a stereomicroscope and cut into fragments of approximately 2 mm^3 for transplantation.

Recipient mice were anesthetized with isoflurane as described above, and a midline laparotomy (approximately 1.5 cm) was performed to expose the abdominal cavity. Isolated endometrial fragments were sutured onto the ventral peritoneal wall at well-vascularized sites using 7 − 0 nylon sutures. The abdominal muscle layer and skin were then closed sequentially with 5 − 0 absorbable sutures. Postoperative care included subcutaneous administration of buprenorphine (0.1 mg/kg) every 12 h for 48 h for analgesia, together with a single intramuscular injection of penicillin G (50,000 IU per mouse) to reduce the risk of infection. Mice were monitored daily for signs of distress or postoperative complications.

Four weeks after transplantation, the abdominal cavity was re-opened and successful model establishment was confirmed by macroscopic observation of fluid-filled cystic lesions attached to the peritoneal wall. Only mice with clearly identifiable ectopic lesions were included in the subsequent intervention studies.

Macrophage culture

The murine macrophage cell line RAW264.7 (ATCC® TIB-71™) was maintained in high-glucose Dulbecco's modified Eagle medium (DMEM; Gibco) supplemented with 10% fetal bovine serum (FBS), 100 U/mL penicillin, and 100 μg/mL streptomycin. Cells were cultured at 37°C in a humidified incubator with 5% CO2 and routinely passaged at 80–90% confluence. All cells were regularly tested and confirmed to be free of mycoplasma contamination.

Isolation and Purification of Migrasomes

To enrich migrasomes from macrophage-conditioned medium, a membrane filtration combined with differential centrifugation method was employed for isolation and purification. RAW264.7 cells were first cultured in DMEM medium supplemented with 10% exosome-free fetal bovine serum for 24 h to induce migrasome release, after which the cell supernatant was collected. The collected supernatant was sequentially centrifuged at 4°C, initially at 1000 × g for 10 min to remove intact cells, and then the resulting supernatant was centrifuged at 4000 × g for 20 min to eliminate dead cells and large debris. Subsequently, the supernatant was filtered through a 0.45 μm pore filter membrane, and migrasomes with larger diameters were retained on the filter membrane. After discarding the filtrate, the membrane was inverted and placed into a new collection tube, covered with an appropriate volume of ice-cold PBS, and centrifuged at 2000 × g for 5 min to elute the captured migrasomes into the solution. The collected eluate served as the enriched migrasome suspension, with a small aliquot used for morphological characterization and protein analysis, while the remainder was aliquoted and stored at − 80°C for further experiments. The isolated migrasomes were identified by scanning electron microscopy, and the expression of the specific marker TSPAN4 was confirmed by Western blot to verify purity.

Scanning Electron Microscopy (SEM)

Migrasome samples were prepared for scanning electron microscopy according to the following protocol. Initially, 1 μL of isolated migrasome suspension was uniformly spread on a clean glass coverslip and allowed to adhere for 2 minutes. The samples were then fixed with 2.5% glutaraldehyde in 0.1 M phosphate buffer (pH 7.4) for 30 minutes at room temperature. Following fixation, samples were rinsed three times with phosphate-buffered saline (PBS), each wash lasting 5 minutes, to remove residual fixative. Dehydration was performed using a graded ethanol series (30%, 50%, 70%, 90%, and 100%) with 15-minute incubation at each concentration. The dehydrated samples were subsequently subjected to critical point drying using a Leica EM CPD300 critical point dryer to preserve ultrastructural integrity. Dried specimens were mounted on aluminum stubs using conductive carbon tape and sputter-coated with a 10-nm gold-palladium layer using a Hitachi E-1045 ion sputter coater to enhance conductivity. Samples were examined using a Hitachi SU8600 cold-field emission scanning electron microscope operated at 5.0 kV. High-resolution images were captured at various magnifications to document migrasome morphology and structural characteristics.

In vivo imaging and migrasome administration

Following successful model establishment, endometriosis-bearing mice were randomly divided into two groups: the migrasome-treated group (n = 5) and the PBS control group (n = 5). Isolated migrasomes (50 μg) were labeled with the near-infrared lipophilic dye DiR at a ratio of 10:1 (w/w) for 30 minutes at 37°C. To remove unbound free dye, the labeled migrasomes were subsequently washed by ultracentrifugation at 100,000 × g for 70 min at 4°C, and the pellet was resuspended in sterile PBS. This washing step was repeated twice to ensure complete removal of residual free DiR. The purified DiR-labeled migrasomes or an equal volume of PBS were administered to the respective groups via intraperitoneal injection. For *in vivo* tracking, mice were imaged using an IVIS Spectrum *in vivo* imaging system (PerkinElmer) at days 1, 2, 4, 6, 8, and 10 post-injection. Fluorescence signals were acquired using an excitation/emission filter set of 745/800 nm. The fluorescence intensity, indicative of migrasome accumulation and retention at the ectopic lesions, was quantified using Living Image software (v.4.5).

Histological sectioning

Ectopic lesions were harvested and immediately fixed in 4% paraformaldehyde (PFA) in 0.1 M phosphate buffer (pH 7.4). Fixation was performed at 4°C for 24 h to minimize tissue autolysis. Subsequently, tissues were thoroughly rinsed under running tap water to remove excess PFA. Dehydration was carried out through a graded ethanol series (70%, 80%, 95%, and 100%), with each step lasting 1–2 h. Tissues were then cleared in two changes of xylene (1 h each) and infiltrated with molten paraffin wax at 60°C in an embedding center (e.g., Leica EG1150) for 2–3 h. After embedding in fresh paraffin, blocks were solidified on a cold plate. Serial sections of 4 μm thickness were cut using a rotary microtrome (Leica RM2235). Ribbons were floated on a 40°C water bath to eliminate wrinkles, collected on poly-lysine-coated glass slides, and dried overnight at 37°C. Prior to staining, sections were deparaffinized in two changes of xylene (10 min each) and rehydrated through a descending ethanol series (100%, 95%, 80%, 70%) to distilled water.

Hematoxylin and Eosin (H&E) Staining

Following deparaffinization and rehydration, tissue sections were stained with Mayer's hematoxylin for 5 min to visualize nuclei. After rinsing in running tap water, sections were differentiated in 1% acid ethanol for 2–3 s and immediately blued in Scott's tap water (or 0.1% ammonia water) for 1 min. After a thorough wash in distilled water, cytoplasmic counterstaining was performed by incubating the sections in eosin Y solution for 3 min. Subsequently, sections were dehydrated through a graded ethanol series (70%, 80%, 95%, and 100%), cleared in two changes of xylene, and mounted with a resinous mounting medium (e.g., neutral balsam or synthetic resin).

Masson's Trichrome Staining

Masson's trichrome staining was performed using a commercial kit according to the manufacturer's instructions with minor adaptations. Briefly, deparaffinized and rehydrated sections were first stained in Weigert's iron hematoxylin working solution for 5 min to label nuclei, followed by washing in running water. Sections were then stained in Biebrich scarlet-acid fuchsin solution for 5–10 min to visualize cytoplasm and muscle fibers. After a brief rinse in distilled water, differentiation was carried out in a

phosphomolybdic-phosphotungstic acid solution for 5 min. Without washing, sections were directly transferred to aniline blue solution for 5 min to stain collagen fibers. Following a quick rinse in distilled water, sections were differentiated in 1% acetic acid for 1 min, dehydrated through an ethanol series, cleared in xylene, and mounted with a synthetic resin. In the resulting images, nuclei appear black, cytoplasm and muscle fibers red, and collagen fibers blue.

Western blot

Total protein was extracted from tissues or cells using ice-cold RIPA lysis buffer supplemented with 1× protease and phosphatase inhibitor cocktail. Protein concentration was determined using a bicinchoninic acid (BCA) assay kit. Equal amounts of protein (20 μg per lane) were separated by 10% SDS-PAGE and subsequently electrotransferred onto polyvinylidene difluoride (PVDF) membranes. After blocking with 5% (w/v) non-fat milk in TBST for 1 h at room temperature, membranes were incubated overnight at 4°C with the following primary antibodies (all from UpingBio, China): anti-phospho-Smad2 (p-Smad2, YP-Ab-01374, 1:2000), anti-Smad2 (YP-Ab-02015, 1:2000), anti-Smad3 (YP-Ab-01173, 1:2000), anti-phospho-Smad3 (p-Smad3, YP-Ab-01340, 1:2000), and anti-α-SMA (α-smooth muscle actin, a widely used commercial antibody, Abcam ab5694, 1:2000). An anti-GAPDH antibody (Proteintech, 60004-1-Ig, 1:5000) was used as a loading control. Following extensive washes with TBST, membranes were incubated with appropriate horseradish peroxidase (HRP)-conjugated secondary antibodies for 1 h at room temperature. Protein bands were visualized using an enhanced chemiluminescence (ECL) substrate and imaged with a chemiluminescence detection system. Band intensity was quantified using ImageJ software.

Immunofluorescence staining

Paraffin-embedded tissue sections were deparaffinized in xylene, rehydrated through a graded ethanol series, and subjected to antigen retrieval by heating in citrate buffer (pH 6.0) or EDTA buffer (pH 9.0) as appropriate for each antibody. After blocking with 5% bovine serum albumin (BSA) in PBS for 1 h at room temperature, sections were incubated overnight at 4°C with the following primary antibodies: anti-E-cadherin (Bioworld, MB66875, 1:50), anti-Vimentin (Bioworld, MB4585, 1:500), anti-CK18 (Bioworld, MB12342, 1:100), anti-TSPAN4 (Abcam, ab230234, 1:100), as well as widely used commercial antibodies against CD163 (Abcam ab182422, 1:200) and CD68 (Abcam ab955, 1:200). After washing, sections were incubated with species-matched Alexa Fluor-488 or -594 conjugated secondary antibodies (1:500) for 1 h at room temperature in the dark. Nuclei were counterstained with DAPI (1 μg/mL) for 5 min. Finally, sections were mounted with anti-fade mounting medium and stored at 4°C in the dark until imaging.

Images were acquired using a Leica SP8 laser scanning confocal microscope under consistent exposure settings. Quantitative analysis of fluorescence intensity and co-localization was performed using ImageJ software with the JACoP plugin. Co-localization was quantified using Manders' overlap coefficient (M1 and M2), which represents the fraction of one signal overlapping with the other.

Enzyme-Linked Immunosorbent Assay (ELISA)

Blood samples were collected from the orbital venous plexus of mice and allowed to clot at room temperature for 30 min. Serum was separated by centrifugation at 3,000 × g for 15 min at 4°C, aliquoted, and stored at -80°C until analysis. Concentrations of TGF-β1, VEGF, and MMP9 in the serum were quantified using specific commercial ELISA kits (R&D Systems DuoSet ELISA kits) strictly according to the manufacturers' protocols. Briefly, 96-well plates pre-coated with capture antibodies were incubated with diluted serum samples and standards in duplicate. After washing, biotinylated detection antibodies and streptavidin-horseradish peroxidase (HRP) conjugate were successively added. The colorimetric reaction was developed using tetramethylbenzidine (TMB) substrate and stopped with 2N H_2SO_4. Absorbance was measured at 450 nm with a reference wavelength of 570 nm using a microplate reader (BioTek Synergy H1). The concentration of each analyte in the samples was interpolated from a standard curve generated using a four-parameter logistic (4-PL) curve fit.

Statistical analysis

All data are expressed as mean ± SEM. Normality was assessed using the Shapiro–Wilk test. Comparisons between two groups were performed using unpaired Student's t-test. Multiple group comparisons were analyzed by one-way or two-way ANOVA followed by Tukey's post hoc test. A p-value < 0.05 was considered statistically significant. All analyses were conducted using GraphPad Prism 9.0 (GraphPad Software, USA).

Abbreviations

Abbreviation	Full Name
α-SMA	alpha-smooth muscle actin
BCA	bicinchoninic acid
CK18	cytokeratin 18
CTGF	connective tissue growth factor
DAPI	4',6-diamidino-2-phenylindole
DMEM	Dulbecco's Modified Eagle Medium
ECL	enhanced chemiluminescence
ECM	extracellular matrix
ELISA	enzyme-linked immunosorbent assay
EMS	endometriosis
EMT	epithelial-mesenchymal transition
EndoMT	endothelial-to-mesenchymal transition
FBS	fetal bovine serum
FMT	fibroblast-to-myofibroblast transdifferentiation
GnRH-a	gonadotropin-releasing hormone agonist
H&E	hematoxylin and eosin
HRP	horseradish peroxidase
IHC	immunohistochemistry
IRB	Institutional Review Board
IVC	individually ventilated cage
MMT	macrophage-to-myofibroblast transition
MMP9	matrix metalloproteinase-9
PBS	phosphate-buffered saline
PDGF	platelet-derived growth factor
PFA	paraformaldehyde
PMA	phorbol 12-myristate 13-acetate
PVDF	polyvinylidene difluoride
SDS-PAGE	sodium dodecyl sulfate-polyacrylamide gel electrophoresis

SEM	scanning electron microscopy / standard error of the mean
SPF	specific pathogen-free
TBST	Tris-buffered saline with Tween 20
TGF-β	transforming growth factor-beta
TMB	tetramethylbenzidine
TSPAN4	tetraspanin 4
VEGF	vascular endothelial growth factor
4-PL	four-parameter logistic

Declarations

Ethics approval and consent to participate

All animal experiments were performed in strict accordance with the National Institutes of Health Guide for the Care and Use of Laboratory Animals (8th edition, 2011) and were approved by the Animal Ethics Committee of Jiangsu University (Approval No. UJS-AEC-2025-14566). The maximal allowable size of ectopic lesions permitted by the committee is 15 mm in diameter. In this study, all ectopic lesions measured at the experimental endpoint were within this limit (mean diameter < 8 mm), and no lesions exceeded the permitted maximal tumor burden. This study did not involve human participants, therefore consent to participate is not applicable.

Consent for publication

Not applicable. This manuscript does not contain any individual person's data in any form (including individual details, images, or videos).

Availability of data and materials

All data generated or analyzed during this study are included in this published article and its supplementary information files. The datasets used and/or analyzed during the current study are available from the corresponding author on reasonable request.

Competing interests

The authors declare that they have no competing interests.

Funding

This work was supported by the Medical Scientific Research Foundation of Jiangsu Commission of Health (Grant No. K2024018), the Young Talent Development Plan of Changzhou Commission (Grant No. CZQM2020117), the Science and Technology Plan Project of Changzhou (Grant No. CJ20243001), the

“14th Five-Year Plan” High-level Talents Training Project of Changzhou (Grant No. 2022CZBJ101) and the Postgraduate Research & Practice Innovation Program of Jiangsu Province (Grant No. KYCX24_3921). The funding bodies played no role in the design of the study, collection, analysis, interpretation of data, or writing of the manuscript.

Authors' contributions

Ye Pan designed the study, performed the experiments, collected and analyzed the data, and drafted the manuscript. Jie Fang and Simeng Zhang performed the animal experiments and collected the data. Peng Lü and Yongbin Ma contributed to the study design and manuscript revision. All authors read and approved the final manuscript.

Acknowledgements

We are thankful to the anonymous reviewers for reviewing our manuscript and providing helpful comments and suggestions.

References

1. Zondervan KT, Becker CM, Koga K, Missmer SA, Taylor RN. Viganò P. Endometriosis. Nat Rev Dis Primers. 2018;4:10.
2. Taylor HS, Kotlyar AM, Flores VA. Endometriosis is a chronic systemic disease: Clinical challenges and novel innovations. Lancet. 2021;397:839–52.
3. Horne AW, Missmer SA. Pathophysiology, diagnosis, and management of endometriosis. BMJ. 2022;379:e070750.
4. Bulletti C, Coccia ME, Battistoni S, Borini A. Endometriosis and infertility. J Assist Reprod Genet. 2010;27:441–7.
5. Zakhari A, Delpero E, McKeown S, Tomlinson G, Bougie O, Murji A. Endometriosis recurrence following post-operative hormonal suppression: A systematic review and meta-analysis. Hum Reprod Update. 2021;27:96–107.
6. Qing X, He L, Ma Y, Zhang Y, Zheng W. Systematic review and meta-analysis on the effect of adjuvant gonadotropin-releasing hormone agonist (gnrh-a) on pregnancy outcomes in women with endometriosis following conservative surgery. BMC Pregnancy Childbirth. 2024;24:237.
7. Filindris T, Papakonstantinou E, Keramida M, Panteris E, Kalogeropoulos S, Georgopoulos N, et al. The effect of gnrh-a on the angiogenesis of endometriosis. Horm (Athens). 2024;23:509–15.
8. Zheng Q, Mao H, Xu Y, Zhao J, Wei X, Liu P. Can postoperative gnrh agonist treatment prevent endometriosis recurrence? A meta-analysis. Arch Gynecol Obstet. 2016;294:201–7.
9. Zondervan KT, Becker CM, Missmer SA, Endometriosis. N Engl J Med. 2020;382:1244–56.
10. Vissers G, Giacomozzi M, Verdurmen W, Peek R, Nap A. The role of fibrosis in endometriosis: A systematic review. Hum Reprod Update. 2024;30:706–50.

11. Kusama K, Tamura K. [fibrosis signaling in endometrial cells and endometriosis development]. Nihon Yakurigaku Zasshi. 2024;159:381–4.
12. Shen M, Liu X, Zhang H, Guo SW. Transforming growth factor β1 signaling coincides with epithelial-mesenchymal transition and fibroblast-to-myofibroblast transdifferentiation in the development of adenomyosis in mice. Hum Reprod. 2016;31:355–69.
13. Wang D, Luo Y, Wang G, Yang Q. Circatrnl1 promotes epithelial-mesenchymal transition in endometriosis by upregulating yes-associated protein 1 in vitro. Cell Death Dis. 2020;11:594.
14. Yan D, Liu X, Xu H, Guo SW. Platelets induce endothelial-mesenchymal transition and subsequent fibrogenesis in endometriosis. Reprod Biomed Online. 2020;41:500–17.
15. Liu S, Li X, Gu Z, Wu J, Jia S, Shi J, et al. Single-cell and spatial transcriptomic profiling revealed niche interactions sustaining growth of endometriotic lesions. Cell Genom. 2025;5:100737.
16. Lv H, Liu B, Dai Y, Li F, Bellone S, Zhou Y et al. Tet3-overexpressing macrophages promote endometriosis. J Clin Invest. 2024;134.
17. Vallvé-Juanico J, Santamaria X, Vo KC, Houshdaran S, Giudice LC. Macrophages display proinflammatory phenotypes in the eutopic endometrium of women with endometriosis with relevance to an infectious etiology of the disease. Fertil Steril. 2019;112:1118–28.
18. Marečková M, Garcia-Alonso L, Moullet M, Lorenzi V, Petryszak R, Sancho-Serra C, et al. An integrated single-cell reference atlas of the human endometrium. Nat Genet. 2024;56:1925–37.
19. Liu Y, Liang S, Yang F, Sun Y, Niu L, Ren Y, et al. Biological characteristics of endometriotic mesenchymal stem cells isolated from ectopic lesions of patients with endometriosis. Stem Cell Res Ther. 2020;11:346.
20. Zhang Z, Wang J, Chen Y, Suo L, Chen H, Zhu L, et al. Activin a promotes myofibroblast differentiation of endometrial mesenchymal stem cells via stat3-dependent smad/ctgf pathway. Cell Commun Signal. 2019;17:45.
21. Stovall DW, Anners JA, Halme J. Immunohistochemical detection of type i, iii, and iv collagen in endometriosis implants. Fertil Steril. 1992;57:984–9.
22. Zhang S, Yang Y, Zhang C, Chen X, Li F, Li J, et al. Spp1 as a key modulator of m2 macrophage polarization promotes endometriosis progression via activation of the fak/pi3k/akt pathway: A bioinformatics and experimental study. Int Immunopharmacol. 2025;166:115563.
23. Ma L, Li Y, Peng J, Wu D, Zhao X, Cui Y, et al. Discovery of the migrasome, an organelle mediating release of cytoplasmic contents during cell migration. Cell Res. 2015;25:24–38.
24. Jiao H, Li X, Li Y, Guo Y, Hu X, Sho T, et al. Localized, highly efficient secretion of signaling proteins by migrasomes. Cell Res. 2024;34:572–85.
25. Strzyz P. Migrasomes promote angiogenesis. Nat Rev Mol Cell Biol. 2023;24:84.
26. Jiang D, He J, Yu L. The migrasome, an organelle for cell-cell communication. Trends Cell Biol. 2025;35:205–16.

27. Jiang Y, Liu X, Ye J, Ma Y, Mao J, Feng D, et al. Migrasomes, a new mode of intercellular communication. Cell Commun Signal. 2023;21:105.
28. Gu C, Chen P, Tian H, Yang Y, Huang Z, Yan H, et al. Targeting initial tumour-osteoclast spatiotemporal interaction to prevent bone metastasis. Nat Nanotechnol. 2024;19:1044–54.
29. Krishnan SR, Bebawy M. Circulating biosignatures in multiple myeloma and their role in multidrug resistance. Mol Cancer. 2023;22:79.
30. Peng Y, Mei S, Qi X, Tang R, Yang W, Feng J, et al. Pgc-1α mediates migrasome secretion accelerating macrophage-myofibroblast transition and contributing to sepsis-associated pulmonary fibrosis. Exp Mol Med. 2025;57:759–74.
31. Cai C, Shen J. The roles of migrasomes in immunity, barriers, and diseases. Acta Biomater. 2024;189:88–102.
32. Tang R, Zhou L, Lin J, Zhang X, Xie P, Zhang L, et al. Migrasome as a novel organelle: Biogenesis, physiological functions, and therapeutic potential. J Transl Int Med. 2026;14:34–52.
33. Hu M, Li T, Ma X, Liu S, Li C, Huang Z, et al. Macrophage lineage cells-derived migrasomes activate complement-dependent blood-brain barrier damage in cerebral amyloid angiopathy mouse model. Nat Commun. 2023;14:3945.
34. Liu W, Li L, Bai X, Zhang M, Lv W, Ma Y, et al. Osteosarcoma cell-derived migrasomes promote macrophage m2 polarization to aggravate osteosarcoma proliferation and metastasis. Adv Sci (Weinh). 2025;12:e2409870.
35. Yu S, Yu L. Migrasome biogenesis and functions. Febs j. 2022;289:7246–54.
36. Jiao H, Li X, Li Y, Guo Z, Yang Y, Luo Y, et al. Packaged release and targeted delivery of cytokines by migrasomes in circulation. Cell Discov. 2024;10:121.
37. Zhang R, Peng J, Zhang Y, Zheng K, Chen Y, Liu L, et al. Pancreatic cancer cell-derived migrasomes promote cancer progression by fostering an immunosuppressive tumor microenvironment. Cancer Lett. 2024;605:217289.
38. Li B, Chen J, Zhu J, Zhou H, Zhang Q, Deng H, et al. M2 macrophage-derived migrasomes mediate ischaemia-induced retinal neovascularization by targeting trem2. J Extracell Vesicles. 2025;14:e70180.
39. Huang Z, Wang M, Chen Y, Tang H, Tang K, Zhao M, et al. Glioblastoma-derived migrasomes promote migration and invasion by releasing pak4 and lama4. Commun Biol. 2025;8:91.
40. Yan C, Sun W, Chen Z, Liu L, Zhou P, Gu Y, et al. Ecm protein cyr61 promotes migration and osteoblastic differentiation of irradiation bmscs via migrasomes. Stem Cells Int. 2025;2025:8825935.
41. Garcia Garcia JM, Vannuzzi V, Donati C, Bernacchioni C, Bruni P, Petraglia F. Endometriosis: Cellular and molecular mechanisms leading to fibrosis. Reprod Sci. 2023;30:1453–61.
42. Chen M, Wang L, Chen Y, Wang T, Jiang G, Chen Q. Integrated analysis of single-cell and bulk transcriptomic data reveals altered cellular composition and predictive cell types in ectopic

endometriosis. Front Med (Lausanne). 2025;12:1641982.
43. Li R, Tran DN, Lessey BA, Young SL, Kim TH, Jeong JW. Transcriptomic changes in eutopic endometrium and ectopic lesions during endometriosis progression in a mouse model. F S Sci. 2024;5:182–94.
44. Wang S, Gu G, Xian X, Li J, Zhang D, Guo J, et al. Cancer cell-derived migrasomes harboring atf6 promote breast cancer brain metastasis via endoplasmic reticulum stress-mediated disruption of the blood-brain barrier. Cancer Biol Med. 2025;22:690–713.
45. Zhao X, Lei Y, Zheng J, Peng J, Li Y, Yu L, et al. Identification of markers for migrasome detection. Cell Discov. 2019;5:27.
46. Chen Y, Li Y, Ma L, Yu L. Detection of migrasomes. Methods Mol Biol. 2018;1749:43–9.

Figures

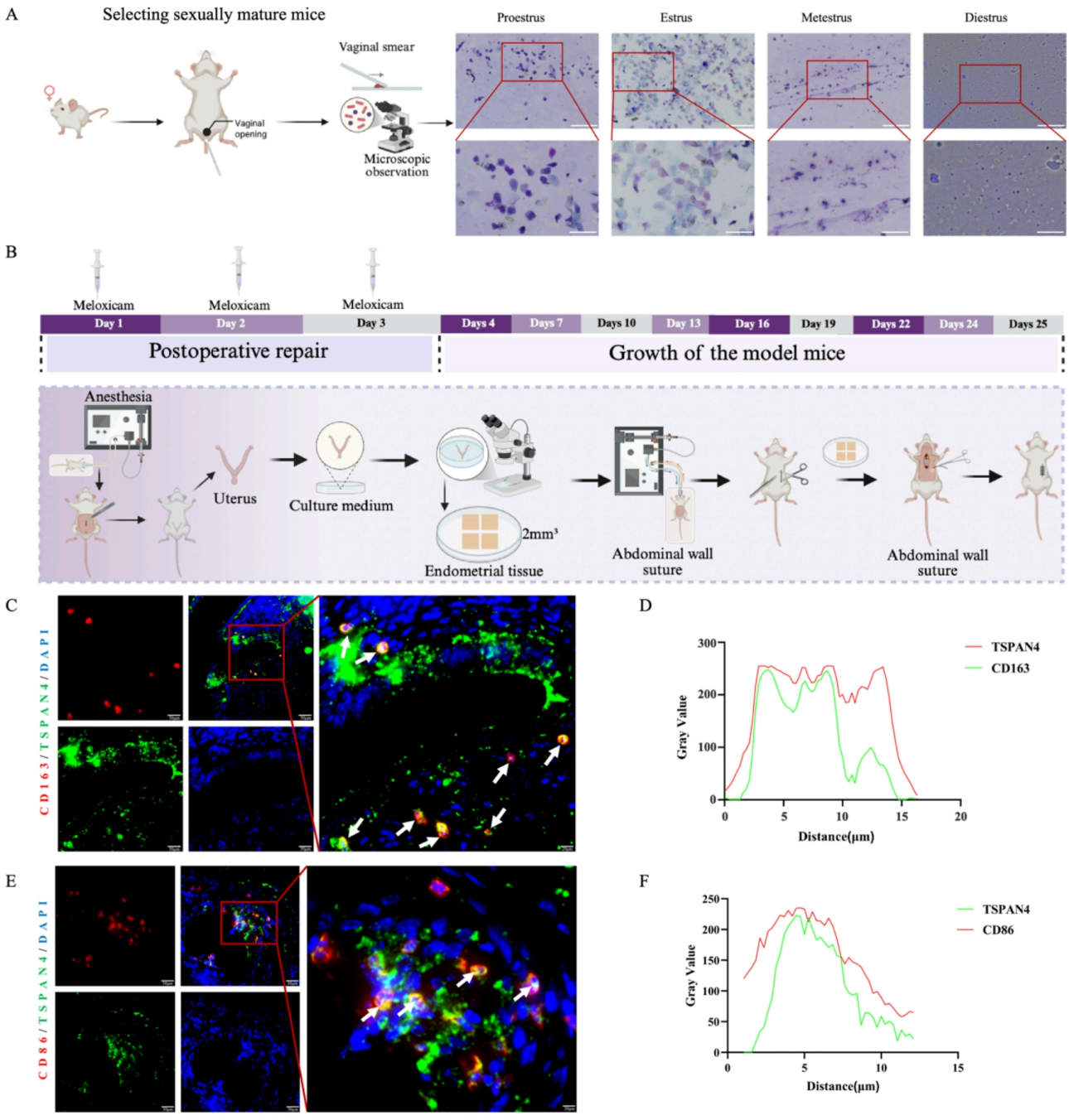


Figure 1

TSPAN4-positive migrasome-like structures are detected in ectopic lesions and show spatial association with infiltrating macrophages in a murine endometriosis model.

(A) Vaginal cytology image showing estrus stage synchronization in mice used for model establishment prior to surgery (scale bar, 50 μm).

(B) Schematic illustration of the murine endometriosis model. Endometrial tissue fragments harvested from donor mice were sutured onto the peritoneal wall of recipient mice to generate ectopic lesions.

(C, E) Multiplex immunofluorescence images of ectopic lesions stained for TSPAN4 (green) and the macrophage-associated markers CD163 (red, C) or CD86 (red, E). Nuclei were counterstained with DAPI (blue). Insets show enlarged views of boxed regions (scale bar, 50 μm). Arrows indicate representative regions of spatial overlap between TSPAN4-positive puncta and macrophage-associated signals.

(D, F) Quantification of colocalization between TSPAN4 and CD163 (D) or CD86 (F) using Manders' overlap coefficients (mean ± SEM; n = 5).

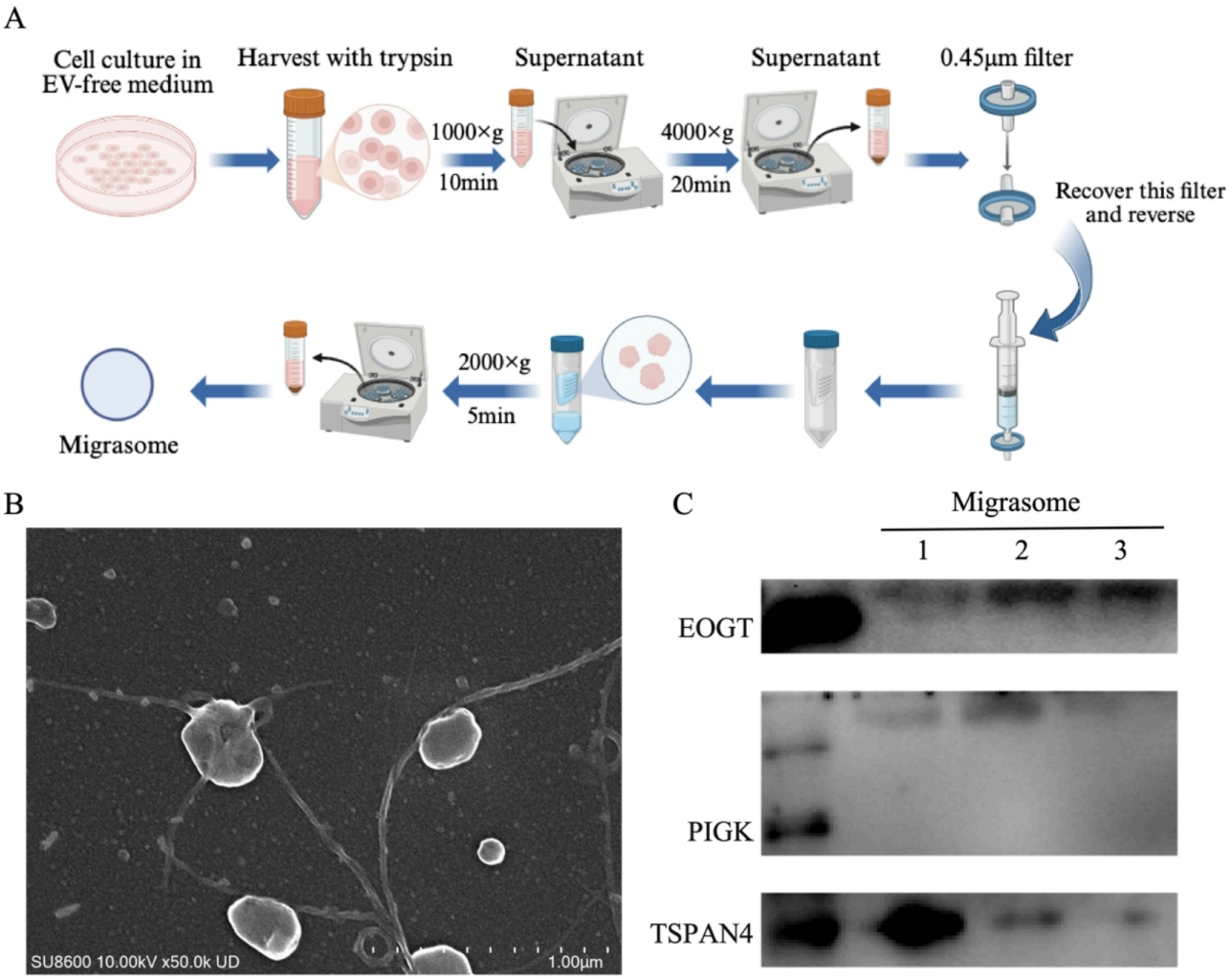


Figure 2

Isolation and characterization of macrophage-derived migrasomes.

(A) Schematic diagram of the migrasome isolation procedure. Cells were cultured in extracellular vesicle depleted medium, and the supernatant was sequentially processed by low-speed centrifugation and membrane filtration to enrich migrasome-containing fractions.

(B) SEM image of the isolated migrasomes (scale bar, 1 μm). It showing large vesicular structures with characteristic migrasome-like morphology, including rounded membrane-bound bodies connected to elongated membranous extensions.

(C) Western blot analysis of migrasome-associated marker proteins. The enriched vesicular fractions showed detectable signals for EOGT, PIGK, and TSPAN4, supporting the molecular identity of the isolated migrasome-enriched preparations. Lanes 1-3 represent independent experimental replicates.

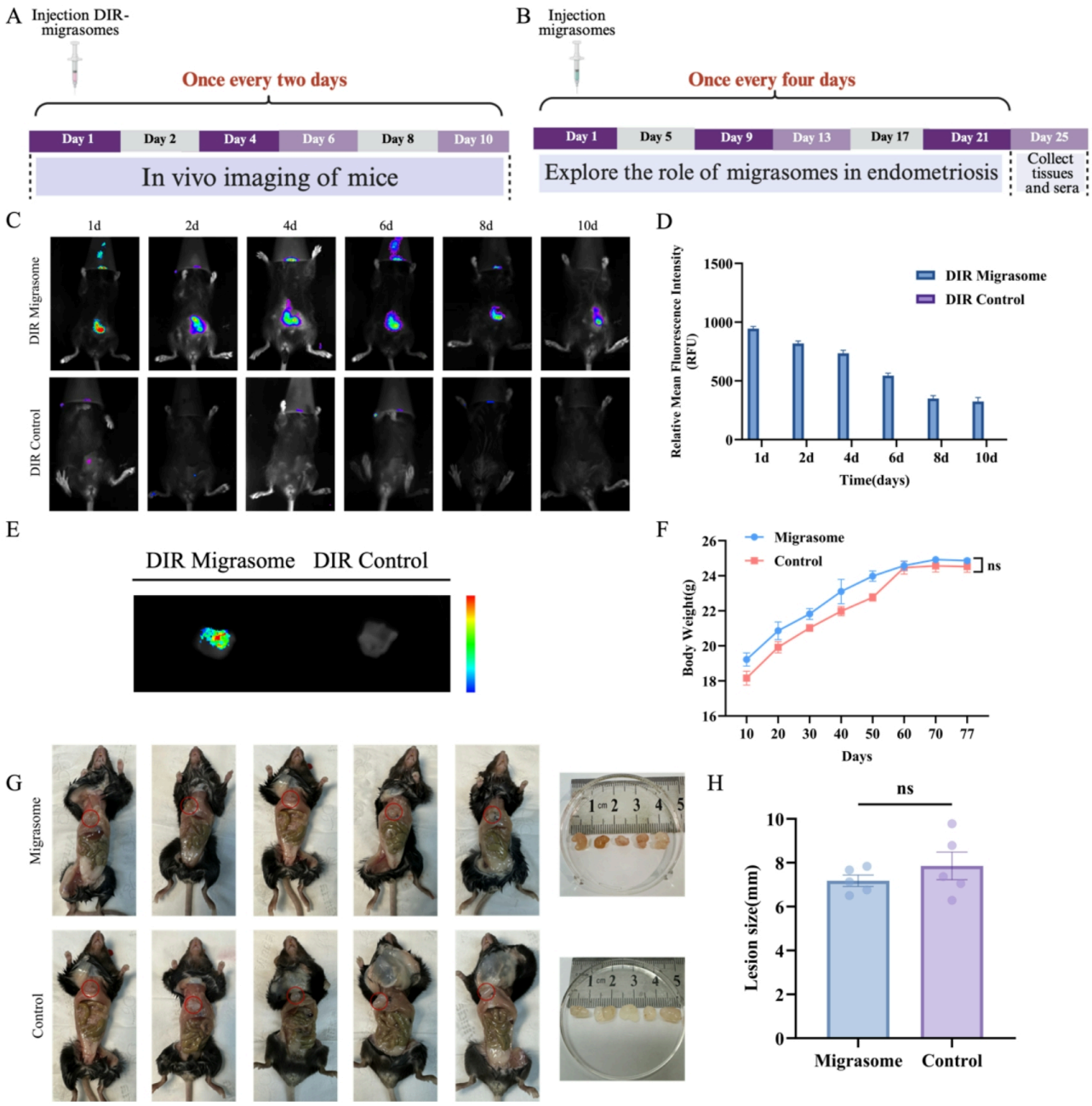


Figure 3

Macrophage-derived migrasomes accumulate in ectopic lesions.

(A) Schematic illustration of the *in vivo* imaging experimental design.

(B) Administration schedule for migrasome treatment.

(C) Representative *in vivo* fluorescence images showing DiR-labeled migrasome accumulation at ectopic lesion sites over time (n = 5).

(D) Quantification of lesion-associated fluorescence intensity (mean ± SEM).

(E) Ex vivo fluorescence analysis of ectopic cysts and major organs at experimental endpoint.

(F) Body weight curves of migrasome-treated and control mice.

(G) Representative photographs of ectopic cysts from control and migrasome-treated mice (n = 5).

(H) Quantitative analysis of cyst diameter (mean ± SEM; ns, not significant).

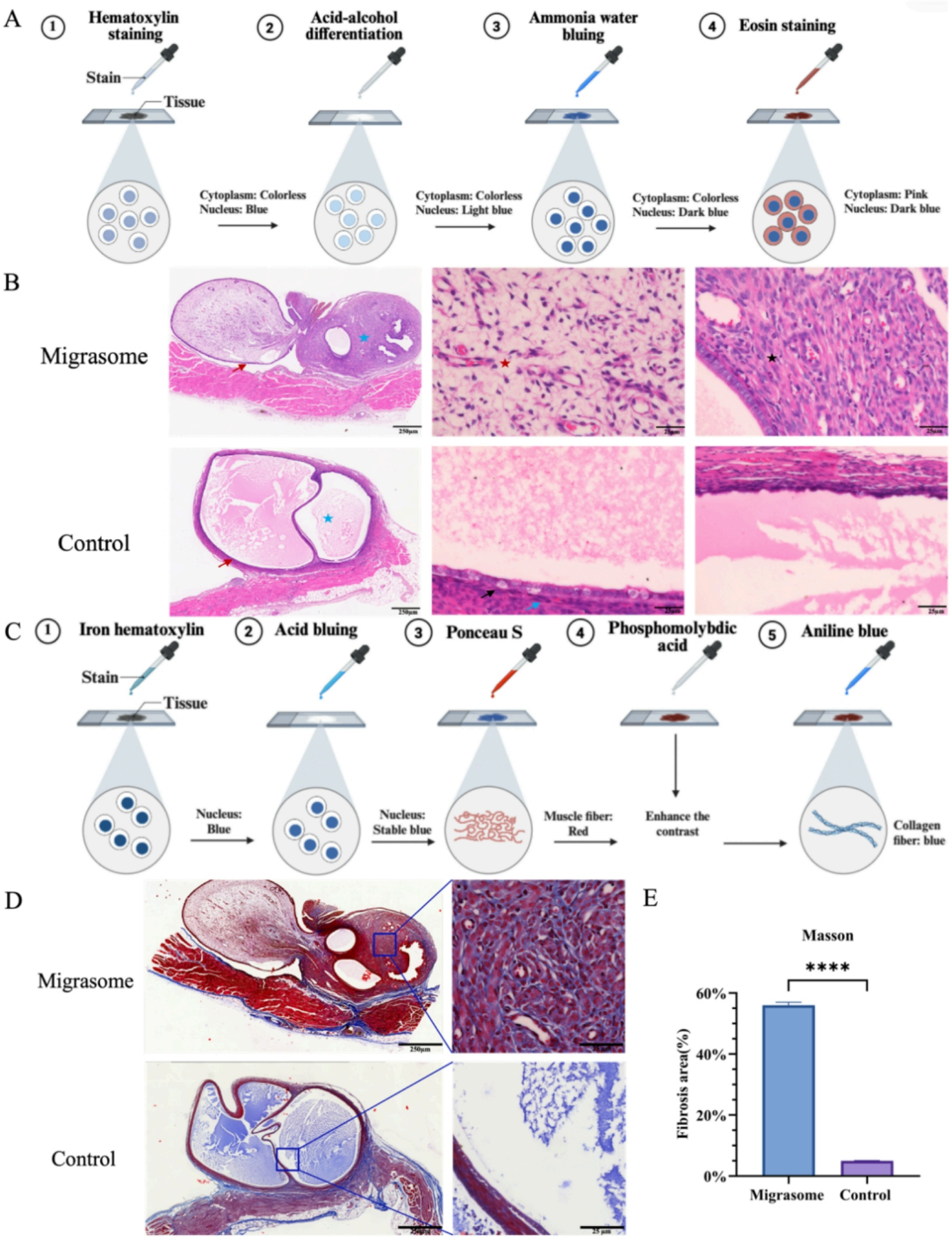


Figure 4

Macrophage-derived migrasomes induce fibrotic remodeling in ectopic lesions.

(A) Schematic illustration of the hematoxylin and eosin (H&E) staining procedure.

(B) Representative H&E-stained sections of ectopic cysts from control and migrasome-treated mice (scale bars, 250 μm and 25 μm).

(C) Schematic illustration of the Masson's trichrome staining procedure.

(D) Representative Masson's trichrome-stained sections of ectopic cysts from control and migrasome-treated mice, with blue indicating collagen deposition (scale bars, 250 μm and 25 μm).

(E) Quantitative analysis of fibrotic area based on Masson's trichrome staining (mean ± SEM; ****$p < 0.0001$; $n = 5$).

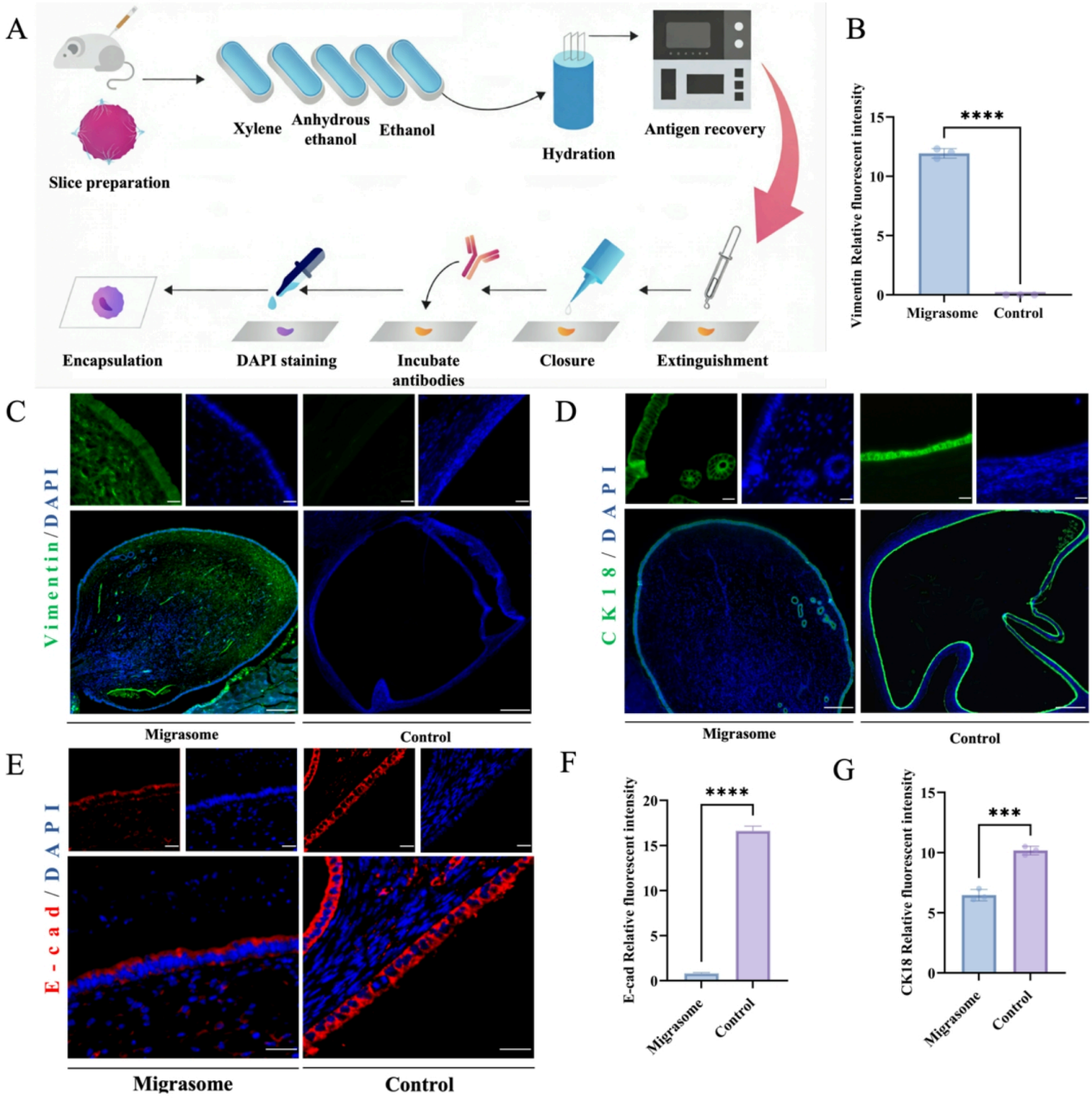


Figure 5

Migrasome treatment is associated with EMT-like phenotypic changes in ectopic lesions.

(A) Schematic illustration of the immunofluorescence staining procedure used for paraffin-embedded ectopic lesion sections, including deparaffinization, antigen retrieval, antibody incubation, nuclear counterstaining, and mounting.

(B) Quantification of vimentin fluorescence intensity in ectopic lesions from migrasome-treated and control groups (mean ± SEM; ****$p < 0.0001$; $n = 5$).

(C) Representative immunofluorescence images of ectopic lesions stained for vimentin (green) with DAPI nuclear counterstaining (blue). Insets show enlarged views of boxed regions (scale bar, 50 μm).

(D) Representative immunofluorescence images of ectopic lesions stained for cytokeratin 18 (CK18) (green) with DAPI nuclear counterstaining (blue). Insets show enlarged views of boxed regions (scale bar, 50 μm).

(E) Representative immunofluorescence images of ectopic lesions stained for E-cadherin (red) with DAPI nuclear counterstaining (blue). Insets show enlarged views of boxed regions (scale bar, 50 μm).

(F) Quantification of E-cadherin fluorescence intensity in ectopic lesions from the migrasome-treated and control groups (mean ± SEM; ****$p < 0.0001$; $n = 5$).

(G) Quantification of CK18 fluorescence intensity in ectopic lesions from the migrasome-treated and control groups (mean ± SEM; ***$p < 0.001$; $n = 5$).

These data show increased vimentin expression together with reduced CK18 and E-cadherin expression in migrasome-treated lesions, consistent with EMT-like phenotypic reprogramming.

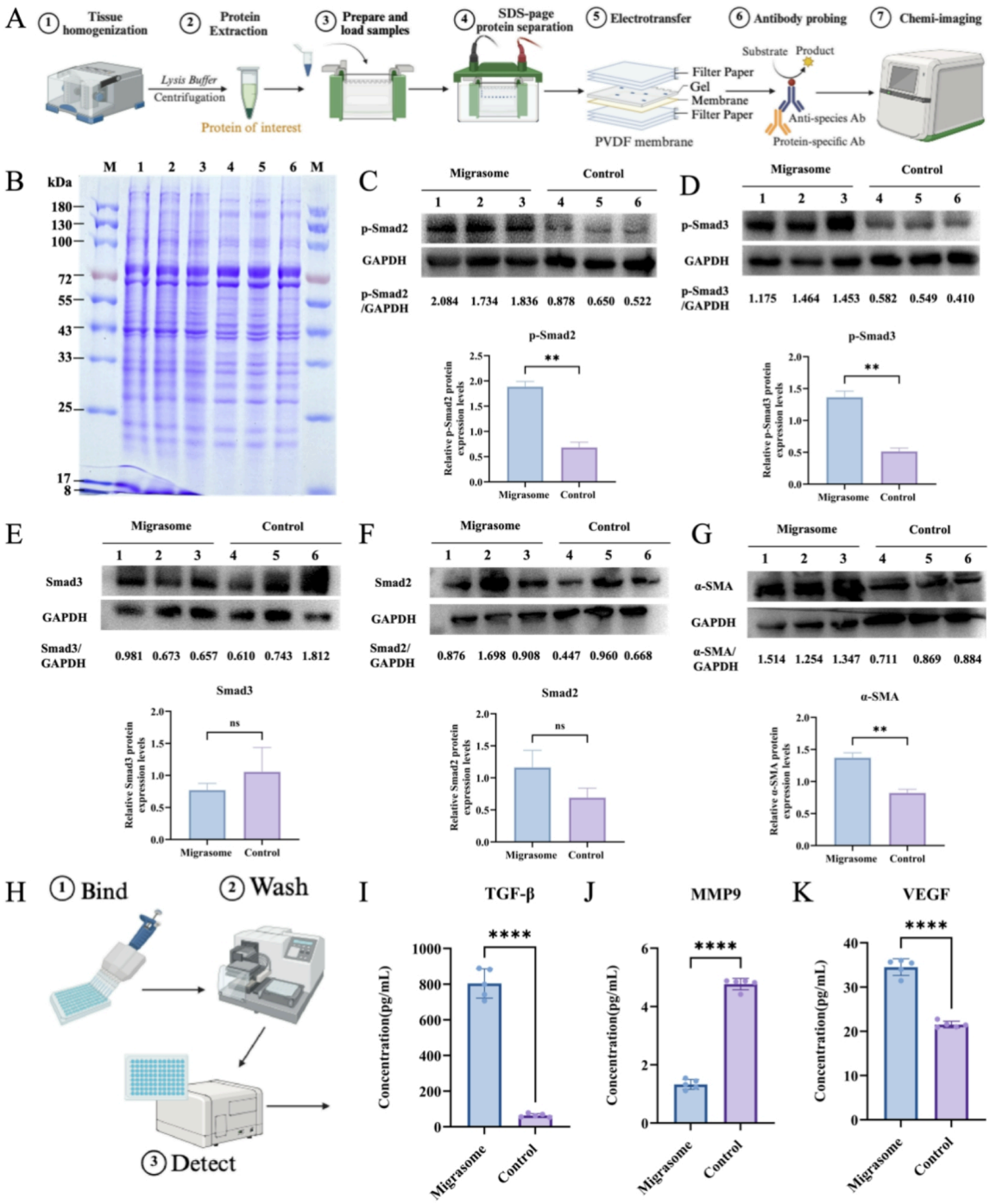


Figure 6

Macrophage-derived migrasomes activate TGF-β/Smad signaling and promote a pro-fibrotic microenvironment.

(A) Schematic illustration of the Western blot experimental workflow.

(B) Coomassie Brilliant Blue-stained SDS-PAGE gel showing protein loading in control and migrasome-treated lesion extracts. Lanes 1-3: Migrasome; Lanes 4-6: Control.

(C–F) Western blot images and quantification of p-Smad2, total Smad2, p-Smad3, and total Smad3 expression in ectopic lesions (mean ± SEM; **p < 0.01; n = 3).

(G) Western blot images and quantification of α-SMA expression (mean ± SEM; **p < 0.01; n = 3).

(H) Schematic illustration of the ELISA procedure.

(I–K) ELISA quantification of active TGF-β1, VEGF, and MMP9 levels in control and migrasome-treated lesions (mean ± SEM; ****p < 0.0001; n = 3).

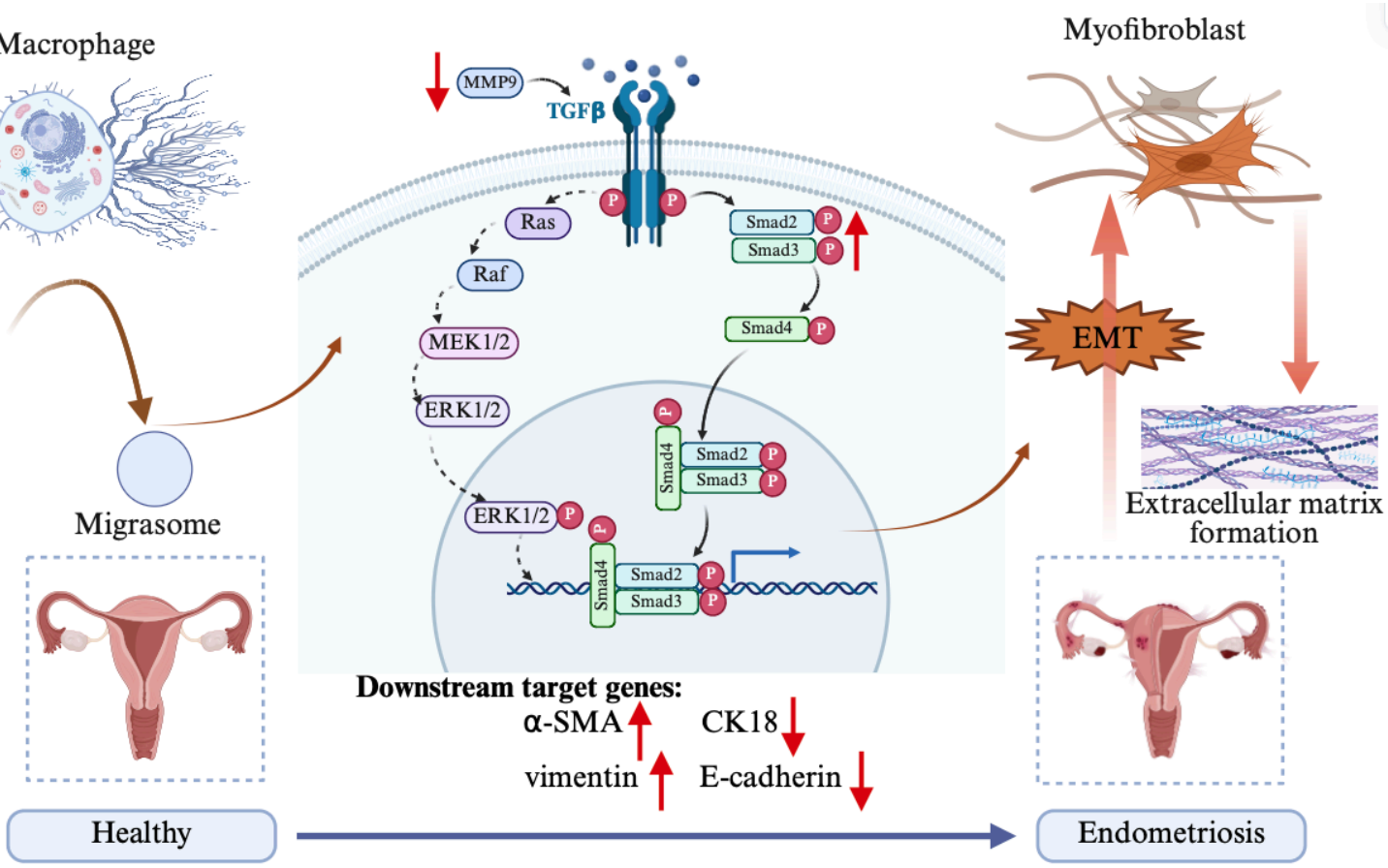


Figure 7

Schematic diagram illustrating the proposed mechanism by which macrophage-derived migrasomes promote fibrosis in endometriosis via activation of the TGF-β/Smad signaling pathway, induction of EMT, and disruption of ECM homeostasis.

Supplementary Files

This is a list of supplementary files associated with this preprint. Click to download.

- SupplementaryMaterials1.docx